



On the performance of the joint velocity-scalar PDF method near walls

Tin-Hang Un ^a,* , Salvador Navarro-Martinez ^{a,b}

^a Department of Mechanical Engineering, Imperial College London, UK

^b I3A and Fluid Mechanics Department, University of Zaragoza, Spain

ARTICLE INFO

Keywords:

Velocity-scalar probability density function (VSPDF)
Eulerian stochastic fields (SF)
Wall-modelled large eddy simulation (WMLES)
Supersonic combustion

ABSTRACT

Wall modelling of turbulent reacting flows is crucial for applications such as aero-engine simulations. The velocity-scalar probability density function (PDF) method has proven effective for modelling flames in complex combustion regimes, but its application near walls is computationally expensive due to the need for wall-resolving grids, even with the aid of adaptive mesh refinement. This study aims to reduce computational cost by employing a modern wall model in large eddy simulations (LES). We demonstrate that a simple subgrid model is sufficient for a wide range of wall distances, though modification to the stochastic forcing is needed to prevent spurious pressure formation near walls. The proposed wall-modelled stochastic fields framework significantly improves upon existing methods without wall modelling. It also highlights the potential for cost savings by using wall-modelled LES-PDF. For this purpose, the Eulerian stochastic fields framework is particularly suited as it can integrate with most existing LES wall models with minimal modifications.

1. Introduction

The joint velocity-scalar probability density function (VSPDF) can be used as a unified framework for modelling turbulent reacting flows [1,2]. It provides closure for all subgrid turbulent transports, turbulence-chemistry interactions, and potentially non-ideal equations of state, without assuming a specific combustion regime or flame structure. Our recent work [3] demonstrated that the VSPDF can effectively model turbulence production and decay in a large eddy simulation (LES) context and can accurately predict autoignition in a supersonic jet flame.

Since most combustion applications occur in confined geometries, accurate prediction of wall-bounded turbulent flow can be of extreme importance to the quantities of interest. However, applying a velocity PDF model near walls is not trivial, as turbulent stresses become highly anisotropic and must follow certain asymptotic scalings close to the wall [4,5]. In high-speed flows, the challenge becomes even more complex due to significant variations in temperature and density [6].

Most attempts to adapt the PDF model near walls focus on modelling the turbulent kinetic energy dissipation rate ϵ in the proximity of solid walls. Early works by Dreeben and Pope [7,8] employed a joint PDF of velocity and frequency. They suggest that $\epsilon \propto u_\tau^3/\kappa y$ and the turbulent length scale $\ell \propto y$ near the wall, where u_τ is the friction velocity, κ is the von Kármán constant, and y is the distance to the wall. They proposed a tensor dissipation term $\varphi_{ij} \propto 1/y$ to account for the non-local effect of fluctuating pressure. The approach was later revised [4]

to include an additional dissipation in the wall-normal velocity component. Their method was adopted by Waclawczyk et al. [5], who proposed a blending function $\propto y$ to switch between the near-wall dissipation model and the standard homogeneous isotropic model.

It is important to note that the above literature considers turbulent stress in the Reynolds-averaged Navier–Stokes (RANS, ensemble average) context. In LES (spatial filter), resolved large eddies capture most anisotropic and non-local effects, and the subgrid stress is expected to return to isotropy much quicker than the RANS stress. Hence, in this work it is postulated that the tensor φ_{ij} is unnecessary and the simpler simplified Langevin model (SLM) [9] would be sufficient in an LES framework. Nevertheless, the model needs to be modified near the wall to ensure that the modelled subgrid kinetic energy behaves correctly.

Another challenge is that previous studies require wall-resolving grids, whose cost is estimated to scale with the Reynolds number $Re^{1.8}$ in LES [10,11], rendering them impractical for many engineering applications. This requirement can be alleviated using hybrid RANS/LES approaches or LES wall models, where the near-wall region is modelled instead of resolved (e.g., see reviews [12–14]). The Eulerian nature of the stochastic fields (SF) PDF formulation [15] allows the direct application of these near-wall modelling strategies. This simplifies the effort to apply the PDF method close to walls and allows a straightforward extension to high-speed flows, e.g., by incorporating the energy equation into an ordinary differential equation (ODE) based wall model [16].

* Corresponding author.

E-mail address: thu17@ic.ac.uk (T.-H. Un).

The present work will extend the VSPDF-SF framework developed in [3] by integrating it with a wall model. The necessary modifications to the model will be discussed, and the solver will be evaluated in high-speed reacting and non-reacting flow cases.

2. Computational models

2.1. Joint velocity-scalar stochastic fields

The well-known closure problem in LES arises when a filtered non-linear function cannot be expressed in terms of the filtered flow quantities, $\overline{Q(\phi)} \neq Q(\overline{\phi})$. This is particularly relevant in highly non-linear chemical reaction source terms. A one-point PDF $f(\boldsymbol{\phi}, \mathbf{x}, t)$ can be defined such that \overline{Q} corresponds to its expected value, *i.e.*,

$$\overline{Q(\boldsymbol{\phi}(\mathbf{x}, t))} = \int_{-\infty}^{\infty} Q(\boldsymbol{\phi})f(\boldsymbol{\phi}; \mathbf{x}, t)d\boldsymbol{\phi}. \quad (1)$$

This equation is exact as long as Q is fully described by the set of variables $\boldsymbol{\phi}$ in the PDF sample space. A joint velocity-scalar PDF with sample space $\boldsymbol{\phi} = [\rho\mathbf{Y}, \mathbf{u}, e]$ covering species' partial densities, velocities, and internal energy, can close the chemical source terms S_α and turbulent transport terms $\overline{\rho u_i u_j}$, $\overline{\rho u_i Y_\alpha}$, $\overline{\rho u_i E}$ without assumptions (where $E = e + u_i u_i / 2$ is the mass-specific total energy).

The PDF is represented by an ensemble of N_f Eulerian stochastic fields (SF), with the discrete version of Eq. (1) being

$$\overline{Q(\boldsymbol{\phi}(\mathbf{x}, t))} \approx \frac{1}{N_f} \sum_{n=1}^{N_f} Q(\boldsymbol{\phi}^{(n)}(\mathbf{x}, t)), \quad (2)$$

where the superscript (n) denotes the solution of the n th SF. Favre filtering \overline{Q} is computed in a similar fashion. Fluctuations about filtered quantities are denoted by Q' and Q'' , such that $Q = \overline{Q} + Q' = \overline{Q} + Q''$.

The SF approach has the advantages of being easy to adapt to existing grid-based LES solvers and ensuring the conservation and boundedness of each stochastic realisation, which is key for numerical stability.

Each field evolves in time following

$$d\mathbf{U}^{(n)} = \left[-\frac{\partial \mathbf{F}_i^{(n)}}{\partial x_i} + \frac{\partial \overline{\mathbf{D}}_i}{\partial x_i} + \mathbf{S}^{(n)} + \rho^{(n)} \mathbf{A}^{(n)} \right] dt + \rho^{(n)} \mathbf{B} d\mathbf{W}^{(n)}, \quad (3)$$

where $\mathbf{U} = [\rho\mathbf{Y}, \rho\mathbf{u}, \rho E]^\top$ are the conservative variables of the Navier–Stokes equation. $\mathbf{F}^{(n)}$ are inviscid Euler fluxes calculated using $\mathbf{U}^{(n)}$; $\overline{\mathbf{D}}$ are the filtered diffusive fluxes; $\mathbf{S}^{(n)}$ are the source terms of $\mathbf{U}^{(n)}$; and $d\mathbf{W}^{(n)}$ are independent Wiener processes non-zero only for the three momentum components.

Interactions between fields are modelled with the drift and stochastic terms. They both average to zero and hence do not alter the filtered values. The drift term A_ϕ reduces subgrid variance inversely proportional to a subgrid turbulence timescale $\tau_{\text{sgs}} = k_{\text{sgs}}/\epsilon_{\text{sgs}}$ [9,17].

$$A_\phi^{(n)} = \frac{C_\phi}{\tau_{\text{sgs}}} (\tilde{\phi} - \phi^{(n)}) \quad (4)$$

for $\phi = Y_\alpha, u_i, e$.

The stochastic term, BdW_i , acts in the opposite manner by increasing the subgrid variance and drives the PDF towards a Gaussian distribution, controlling the rate of return to isotropy,

$$B = \sqrt{C_0 \epsilon_{\text{sgs}}}. \quad (5)$$

Note that the stochastic term is only applied to the momentum components.

The subgrid dissipation rate ϵ_{sgs} is modelled as a function of the subgrid kinetic energy $k_{\text{sgs}} = \overline{u_i'' u_i''} / 2$,

$$\epsilon_{\text{sgs}} = C_\epsilon \left(1 + M_{\text{sgs}}^2 \right) \frac{k_{\text{sgs}}^{3/2}}{\ell}, \quad (6)$$

with the subgrid Mach number $M_{\text{sgs}} = \sqrt{2k_{\text{sgs}}/\bar{c}}$ accounts for the effect of dilatational dissipation in compressible turbulence [18], where \bar{c} is the local speed of sound. The length scale ℓ is chosen to be the local LES filter width Δ . The model constants are $C_0 = 2.1$, $C_\epsilon = 1.05$, $C_u = (1/2 + 3C_0/4)$, and $C_e = C_Y = 1$ following [9,17–20].

2.2. Wall fluxes model

The boundary layer is a thin region near a wall where a steep velocity gradient exists as a result of the no-slip condition. Its profile is self-similar with respect to the non-dimensional distance and velocity, $y^+ = yu_\tau \rho_w / \mu_w$ and $u^+ = u/u_\tau$, where $u_\tau = \sqrt{\tau_w / \rho_w}$ is the friction velocity, and ρ_w , μ_w , τ_w , are density, dynamic viscosity, and shear stress at the wall ($y = 0$), respectively. A wall-resolved LES requires the first grid point to be positioned at $y^+ \approx 1$. As u_τ increases with Re , the number of grid points required to maintain this condition grows quickly. Alternatively, wall-modelled LES strategies leverage some universality of the boundary layer to model, instead of resolve, the near-wall region. Therefore, the grid-point requirement is only bounded by the outer turbulence scales. The cost savings can be up to several orders of magnitude, especially when Re is high [11].

In this work, we utilise the equilibrium wall stress model by Kawai & Larsson [16] where two coupled ODEs are solved on a one-dimensional virtual domain normal to the wall. The virtual domain is embedded in the LES grid, which takes the LES solution as boundary conditions at the far end, and no-slip adiabatic or isothermal wall conditions on the wall end. The outputs are wall shear stress τ_w and heat flux q_w , which, in turn, are used to update the LES flow field.

$$\frac{d}{dy} \left[(\mu + \mu_t) \frac{du_{\parallel}}{dy} \right] = 0, \quad (7)$$

$$\frac{d}{dy} \left[(\mu + \mu_t) u_{\parallel} \frac{du_{\parallel}}{dy} + (\lambda + \lambda_t) \frac{dT}{dy} \right] = 0, \quad (8)$$

where d/dy denotes wall-normal derivative, and u_{\parallel} is the wall-parallel velocity. Turbulent viscosity and conductivity are modelled following [16],

$$\mu_t = \kappa \rho u_\tau y \left[1 - \exp\left(-\frac{y^+}{A^+}\right) \right]^2, \quad \lambda_t = \frac{c_p \mu_t}{Pr_t}. \quad (9)$$

The parameters are $\kappa = 0.41$, $Pr_t = 0.9$, $A^+ = 17$ following [16]. The second LES cell from the wall is used as the matching point of the virtual domain (the far end), as suggested by [16]. Eq. (7)–(8) are applied to the mean/filtered flow quantities, and all stochastic fields share the same τ_w and q_w . This allows the formulation to stay consistent with the filtered diffusive fluxes in Eq. (3) in the limit of the wall.

2.3. Near-wall treatments for the PDF

While the wall stress model accurately captures the mean flow, additional measures are required to ensure the proper behaviour of subgrid quantities near walls. If we follow [7], in the logarithmic layer,

$$k \propto -\langle uv \rangle \propto u_\tau^2, \quad (10)$$

$$\epsilon = \mathcal{P} = -\langle wv \rangle \frac{u_\tau}{\kappa y} \propto \frac{k^{3/2}}{\kappa y}, \quad (11)$$

where angled brackets and \cdot denote RANS averaging and the fluctuations around it.

These relationships were originally discussed in a RANS context. *A priori* analysis by filtering the DNS turbulent channel flows by Lee et al. [21] reveals that although Eq. (10) is true for LES, Eq. (11) is not. Therefore, even though $k_{\text{sgs}}^{3/2}/\kappa y$ follows accurately the production-like term $\hat{P}_{\text{sgs}} = \overline{u'v'u_\tau/\kappa y}$, it fails to model ϵ_{sgs} as intended.

Surprisingly, Fig. 1 shows that the ϵ_{sgs} model in Eq. (6), assuming isotropic flow, agrees well with DNS across the whole range of y^+ in

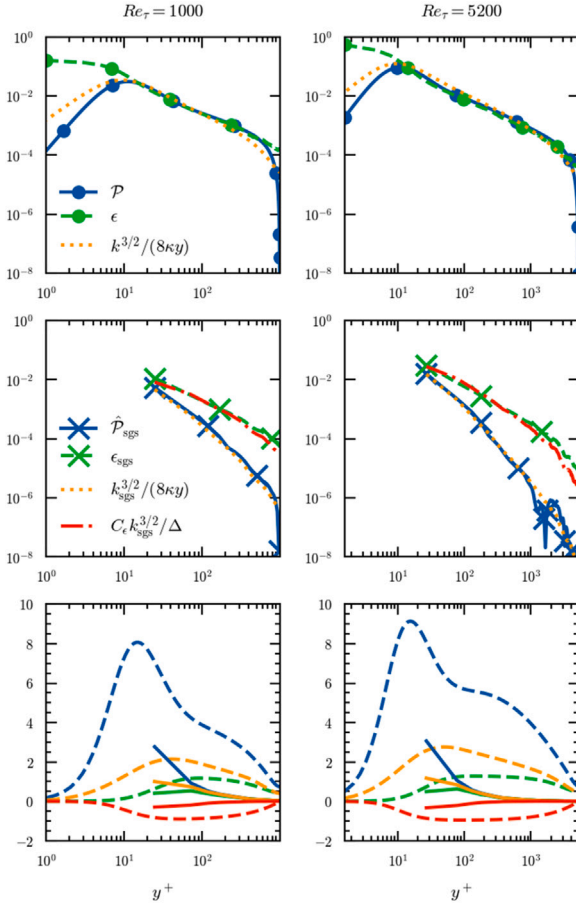


Fig. 1. Top row: Production (\mathcal{P}) and dissipation (ϵ) of turbulent kinetic energy (k) in RANS, along with Eq. (11); Middle row: Production-like $\hat{\mathcal{P}}_{\text{sgs}}$ and dissipation (ϵ_{sgs}) of subgrid kinetic energy (k_{sgs}) in LES ($\Delta^+ \approx 50$), along with Eq. (6) and (11); Bottom row: Reynolds stress (dash line) and subgrid stress (solid line) normalised by u_τ , in descending order of the peak value, $u'u'$, $v'v'$, $w'w'$, $u'v'$, respectively.

both Re_τ tested. This can be explained physically by the fact that even if ℓ decreases with y , C_ϵ also changes, and the two effects cancel out each other.

Another key observation is that LES subgrid stresses are significantly smaller than RANS stresses and return to isotropy much more rapidly. This suggests that in LES, the resolved large eddies primarily capture the flow anisotropy, while the subgrid scales align more closely with Kolmogorov's hypothesis. As a result, the applicability of the simple model is substantially extended.

Another requirement for the model is that $C_0 \rightarrow 0$ as $y \rightarrow 0$ [7]. This represents the realisability constraint of the Reynolds stress tensor. More importantly, the stochastic forcing $\sqrt{C_0} \epsilon dW_i$ normal to the wall must vanish approaches the wall to satisfy the non-permissible condition. If this is not done, spurious pressure waves will form, as shown in Section 3.1. We choose C_0 to decay linearly with y ,

$$C_0 = \min(2.1, y^+/250). \quad (12)$$

The constant 250 is empirically calibrated from the supersonic channel flow in Section 3.1. Additionally, for numerical stability, $C_0 = 0$ is applied to the two cells closest to the wall. This is consistent with the region where the wall stress model is applied.

Table 1
Summary of simulation parameters [27].

Parameter [unit]	Value
Bulk Reynolds number $Re_b = \frac{\rho_w u_b h}{\mu_w}$ [-]	17 000
Bulk Mach number $M_b = \frac{u_b}{c_w}$ [-]	1.5
Friction velocity u_τ [cm/s]	2913.43
Wall temperature T_w [K]	500
Wall dynamic viscosity μ_w [g/cm-s]	2.67×10^{-4}
Channel half height h [cm]	0.6845
Domain size L_x, L_y, L_z [cm]	$12h, 2h, 4h$
Mesh size N_x, N_y, N_z [-]	192, 32, 64

2.4. Implementation

All simulations presented were conducted using the in-house finite difference solver, Cerisse [22]. It is implemented based on AM-ReX [23], which provides efficient block-structured grid adaption routines. The inviscid fluxes are reconstructed using a fifth-order Targeted-Essentially-Non-Oscillatory (TEN0) scheme [24] and an HLLC Riemann solver [25]. Diffusive fluxes are discretised using second-order central difference, with mixture-rule species diffusivity [26].

Time integration is carried out using a second-order explicit Runge-Kutta scheme with operator-splitting procedures. When τ_{sgs} is small or ϵ_{sgs} is large, the subgrid model places a stringent requirement on the time step size, analogous to the CFL condition. It can be circumvented using a novel two-step integration procedure

$$\Delta u_i^* = B \Delta W, \quad (13)$$

$$\begin{aligned} \Delta u_i &= \int_t^{t+\Delta t} A_{u_i} dt + B \Delta W \\ &\approx \Delta u_i^* + \frac{(\tilde{u}_i - u_i^{(n)} - \Delta u_i^*) \Delta t}{\Delta t + \tau_{\text{sgs}}/C_{u_i}}. \end{aligned} \quad (14)$$

ΔW is a dichotomic random number with variance Δt . See [3] for full details on the solver implementation and discussions regarding the use of adaptive mesh refinement (AMR) with SF.

3. Results

3.1. Supersonic turbulent channel flow

The supersonic turbulent channel flow of Modesti & Pirozzoli [27] is used to test the wall-modelled SF strategy. The case parameters are listed in Table 1. LESs with the WALE model [28] are used for a comparative assessment with SF. The WALE model is designed to provide the correct near-wall scaling of the eddy viscosity without requiring a dynamic procedure. It can be coupled with the same ODE wall model presented. All simulations share the same mesh and numerical schemes, with $y^+ = 32$ for the first LES grid point.

Due to the coarse near-wall resolution, LES without wall model underpredicts both τ_w and q_w , leading to an overestimated bulk velocity $\langle u \rangle$ and temperature $\langle T \rangle$, as shown in Fig. 2. Applying the wall model greatly improves the results. The SF predicts a lower $\langle T \rangle$ both with and without wall model, by approximately 5% compared to WALE. The exact reason behind this phenomenon remains unclear, but speculation is around the lower density near the walls compared to the WALE model. Furthermore, SF without the wall model and the C_0 modification performs worse than other approaches and deviates further from DNS, especially in density, showcasing the importance of modifying C_0 .

The root-mean-square (RMS) velocities for all simulations agree well with DNS results, even in the absence of a wall model. This suggests that the RMS values are less sensitive to wall stress than the mean values. However, discrepancies are observed within a few grid points from the wall. This is somewhat expected because, even if τ_w is

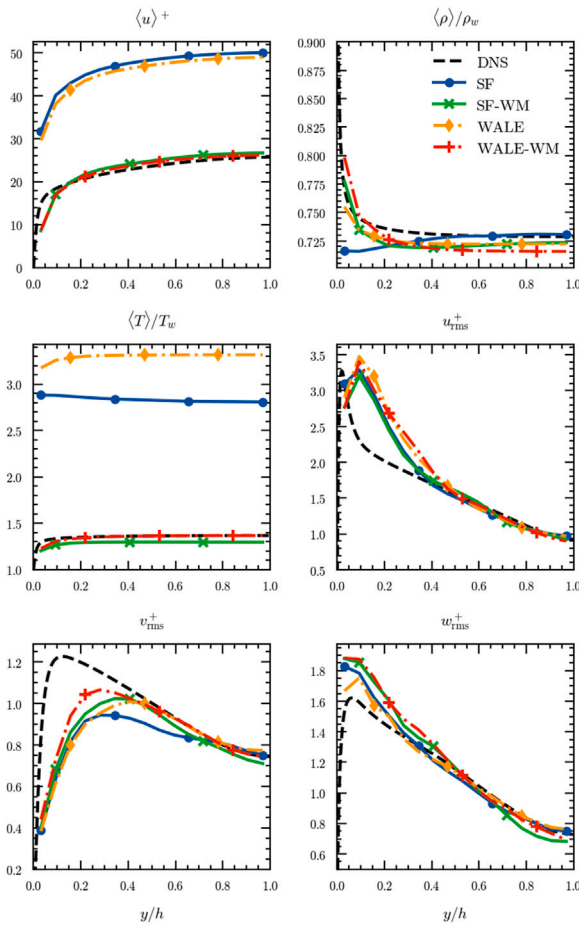


Fig. 2. Mean and root-mean-square profiles. Labels are “DNS”: DNS from [27]; “SF”: SF w/o wall model; “SF-WM”: SF w/ wall model; “WALE”: WALE w/o wall model; “WALE-WM”: WALE w/ wall model.

predicted correctly, the grid is too coarse to capture the small eddies in the boundary layer.

The direct effect of C_0 can be seen in Fig. 3. Without the modification in Eq. (12), non-zero C_0 in the stochastic term creates a forcing in the wall-normal direction, generating spurious pressure waves that contaminate the SF solution. After applying the C_0 modification, the pressure fields are smoother and exhibit less fluctuations.

The effect of the number of fields is examined in Fig. 4. The prediction of $\langle T \rangle$ improves with more fields, but the overall difference remains small. Similarly, the shape and magnitude of k_{sgs} vary slightly. It is difficult to assess the predictions of k_{sgs} , as they are not available in the literature and are mesh (or filter) dependent. Nevertheless, the SFs with wall model produced k_{sgs} that follows the general trend, as observed in Fig. 1, whereas the SF without wall model fails to replicate it.

3.2. Michigan ramjet

With the velocity PDF validated in the canonical flow case, we apply the full velocity-scalar PDF to a laboratory-scale ramjet experimentally studied by Micka [29] (see Table 2). The complex flow patterns in this configuration are characterised by: (1) shock/boundary layer interactions (SBLI) and shock train induced by the combustor back pressure, (2) high-speed fuel injection into a crossflow, and (3) flame stabilised in the jet wake, making this case ideal for validating the model in a multi-physics engineering scenario.

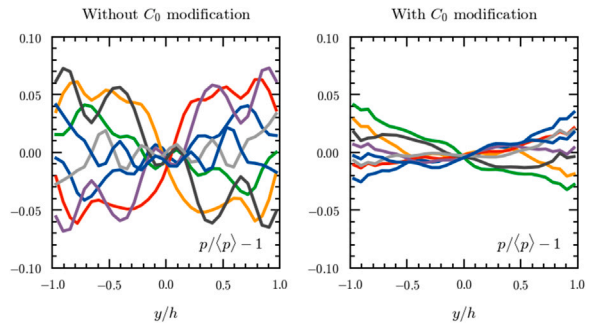


Fig. 3. Pressure of individual fields with and without near-wall C_0 modification (Eq. (12)). Each line represents one SF.

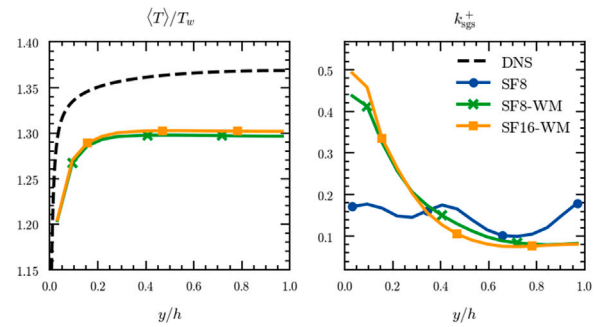


Fig. 4. Comparison between 8 and 16 stochastic fields.

Table 2

Inflow and fuel injection parameters [29].

Parameter [unit]	Value
Inflow Mach number M [-]	2.2
Inflow stagnation temperature T_0 [K]	1400
Inflow stagnation pressure p_0 [kPa]	590
Fuel Mach number M [-]	1
Fuel stagnation temperature T_0 [K]	288
Fuel stagnation pressure p_0 [kPa]	755
Global equivalence ratio (H_2 -air) [-]	0.28

Based on the inflow conditions and isolator height, the Reynolds number is $Re \approx 10^7$. Due to the short residence time, a detailed chemical mechanism is necessary for correctly predicting autoignition and the flame position. A 9-species, 21-reaction H_2 -air mechanism by Li et al. [31] is used, which has been successfully applied in DNS of a similar configuration [32].

Eight SF are employed as a compromise between accuracy and computational cost, which is also in line with usual practice [3]. Two levels of refinement are used, with the finest mesh size being 0.03 cm. The grid is adaptively refined around regions of high pressure gradient and vorticity to capture shocks and mixing. The average y^+ of the first grid point is approximately 200. The resulting total cell count is 8.3 million. This is estimated to be approximately one-tenth of the cell count of a wall-resolved LES.

Results are compared to an implicit LES (ILES) where numerical dissipation serves as the turbulence model, neglecting subgrid fluctuations. In Fig. 5, the instantaneous temperature field shows the presence of a shock train that begins approximately 30 cm ahead of the fuel injector. A shock was initially formed in the combustor as a result of the pressure rise due to combustion. It then travels upstream and stabilises into a classical SBLI configuration, with 4–5 consecutive, increasingly weaker shocks, gradually bringing the flow to subsonic speeds. This flow structure is not present in the simulation without the wall model. This is because when shear stress is underpredicted, the boundary layer

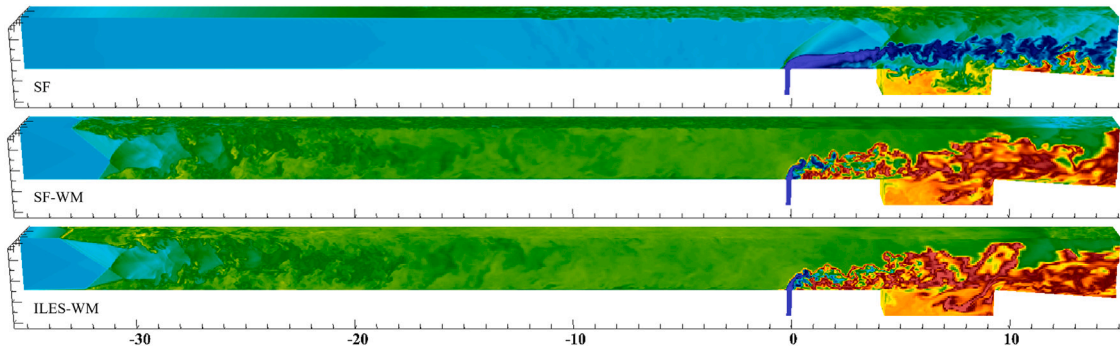


Fig. 5. Instantaneous temperature field of SF with C_0 modification but without wall model (top), SF with both C_0 modification and wall model (middle), and ILES with wall model (bottom). All plots have the same colourmap ranging from 200 K to 2500 K.

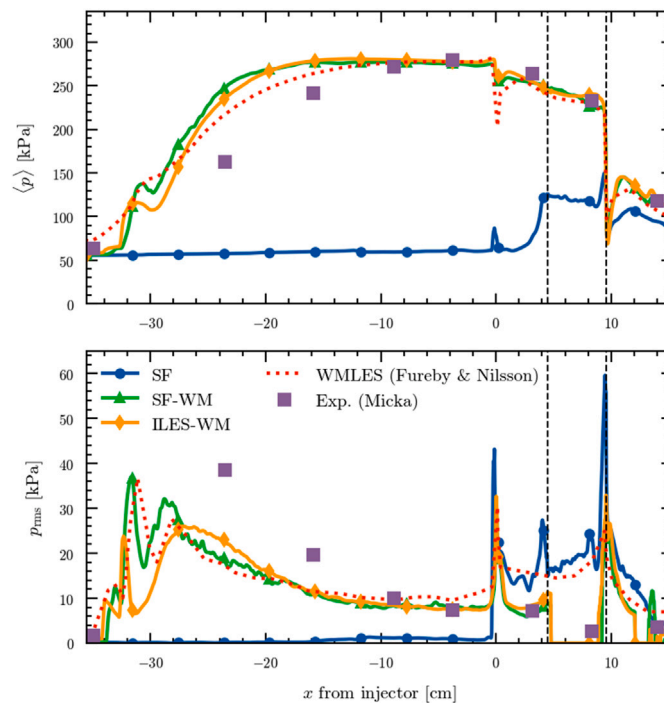


Fig. 6. Mean and RMS values of bottom wall pressure. The dashed lines mark the cavity location. Labels are the same as Fig. 5, while “WMLES” is the wall-modelled LES in [30], and “Exp.” is the experimental measurements in [29].

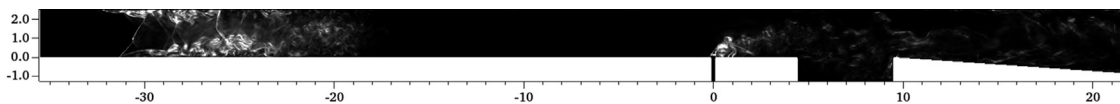


Fig. 7. Subgrid kinetic energy distribution of wall-modelled SF at the centre plane. Brighter indicates higher k_{sgs} .

grows much slower and cannot provide sufficient room for the back pressure to transmit upstream, hence preventing the formation of the shock train. As a result, the flow remains supersonic throughout the isolator, and a bow shock is formed at the fuel jet and a weak flame is stabilised in the cavity. The wall pressure distribution in Fig. 6 confirms that the wall-modelled SF and ILES agree well with experimental measurements and previous wall-modelled LES study [30], while the simulation without wall modelling is inaccurate.

Concerning the effect of small scales, it can be seen in Fig. 7 that k_{sgs} from the wall-modelled SF peaks at two locations: the separation bubble of the first shock and the fuel injection point. However, due

to the length of the isolator, most of the k_{sgs} decays before reaching the fuel injector. Therefore, the shock train’s impact on fuel mixing is mainly done through resolved scales rather than subgrid scales.

Since the flow has been slowed and heated substantially in the isolator, ignition takes place once the hydrogen is mixed with air shortly after injection. In this case, the flame is primarily controlled by large-scale mixing, and the chemical reactions happen quickly due to the high temperature, so the influence of SF is not significant. Nevertheless, the proposed wall-modelled SF approach is successfully validated in this complex and challenging flow field, demonstrating its

potential for efficient applications of the PDF method in wall-bounded flow configurations.

4. Conclusions

This paper presents a wall-modelled stochastic fields (WMSF) strategy as a straightforward and efficient extension for applying the joint velocity-scalar PDF to wall-bounded flows.

The primary objective of this approach is to reduce the high computational costs associated with resolving viscous length scales close to solid walls. This is achieved by coupling the SF with a state-of-the-art wall stress model that can accurately predict shear stress and heat flux. The Eulerian stochastic fields approach simplifies the implementation of most existing wall models, with the potential of applying more advanced wall models with PDF methods in the future.

The results show that the simplified Langevin model, originally designed for isotropic flow, can effectively predict subgrid-scale dissipation across a wide range of y^+ values. Modification to the stochastic term in the SF momentum equation is required to ensure it vanishes near the wall, preventing spurious pressure generation.

The resultant WMSF framework is validated in a supersonic turbulent channel flow and a ramjet case, showing good agreement with DNS and experimental data, and demonstrating the method's versatility for complex flow cases.

This new approach represents a significant improvement over the SF without wall modelling, thereby enabling accurate simulations of wall-bounded turbulent reacting flows at a reasonable computational cost.

Novelty and significance statement

The novelty of this research is that it is the first attempt to integrate a modern LES wall model into the LESPDF approach. It is significant as it unlocks the potential of applying the velocity-scalar PDF in wall-bounded flows, as well as to perform wall-modelled LES with the PDF, which represents an order-of-magnitude cost saving compared to wall-resolved LES. The study also investigates the applicability of the existing simplified Langevin model in the LES context, while many previous works focus on RANS modelling. Even for previous LES-PDF works, discussions contrasting the LES with RANS are not usually given. The results of this work demonstrate a significant improvement achieved by employing an ODE-based wall model. The Eulerian stochastic field formulation is especially well-suited for implementing such models without requiring extensive modifications.

Declaration of competing interest

The authors declare that they have no known competing financial interests or personal relationships that could have appeared to influence the work reported in this paper.

References

- [1] D. Haworth, Progress in probability density function methods for turbulent reacting flows, *Prog. Energy Combust. Sci.* 36 (2010) 168–259.
- [2] Y. Almeida, S. Navarro-Martinez, Joint-velocity scalar energy probability density function method for large eddy simulations of compressible flow, *Phys. Fluids* 33 (2021) 035155.
- [3] T.-H. Un, S. Navarro-Martinez, Stochastic fields with adaptive mesh refinement for high-speed turbulent combustion, *Combust. Flame* 272 (2025) 113897.
- [4] T.D. Dreeben, S.B. Pope, Probability density function/Monte Carlo simulation of near-wall turbulent flows, *J. Fluid Mech.* 357 (1998) 141–166.
- [5] M. Wacławczyk, J. Pozorski, J.-P. Minier, Probability density function computation of turbulent flows with a new near-wall model, *Phys. Fluids* 16 (2004) 1410–1422.
- [6] X.I. Yang, J. Urzay, S. Bose, P. Moin, Aerodynamic heating in wall-modeled large-eddy simulation of high-speed flows, *AIAA J.* 56 (2018) 731–742.
- [7] T.D. Dreeben, S.B. Pope, Wall-function treatment in pdf methods for turbulent flows, *Phys. Fluids* 9 (1997) 2692–2703.
- [8] T.D. Dreeben, S.B. Pope, Probability density function and Reynolds-stress modeling of near-wall turbulent flows, *Phys. Fluids* 9 (1997) 154–163.
- [9] D.C. Haworth, S.B. Pope, A generalized langevin model for turbulent flows, *Phys. Fluids* 29 (1986) 387–405.
- [10] U. Piomelli, Wall-layer models for large-eddy simulations, *Prog. Aerosp. Sci.* 44 (2008) 437–446.
- [11] H. Choi, P. Moin, Grid-point requirements for large eddy simulation: Chapman's estimates revisited, *Phys. Fluids* 24 (2012).
- [12] P.R. Spalart, Detached-eddy simulation, *Annu. Rev. Fluid Mech.* 41 (2009) 181–202.
- [13] J. Larsson, S. Kawai, J. Bodart, I. Bermejo-Moreno, Large eddy simulation with modeled wall-stress: recent progress and future directions, *Mech. Eng. Rev.* 3 (2016) 15–00418.
- [14] S.T. Bose, G.I. Park, Wall-modeled large-eddy simulation for complex turbulent flows, *Annu. Rev. Fluid Mech.* 50 (2018) 535–561.
- [15] L. Valiño, A field Monte Carlo formulation for calculating the probability density function of a single scalar in a turbulent flow, *Flow Turbul. Combust.* 60 (1998) 157–172.
- [16] S. Kawai, J. Larsson, Wall-modeling in large eddy simulation: Length scales, grid resolution, and accuracy, *Phys. Fluids* 24 (2012).
- [17] C. Dopazo, Probability density function approach for a turbulent axisymmetric heated jet. Centerline evolution, *Phys. Fluids* 18 (1975) 397–404.
- [18] B.J. Delarue, S.B. Pope, Application of PDF methods to compressible turbulent flows, *Phys. Fluids* 9 (1997) 2704–2715.
- [19] S.B. Pope, Transport equation for the joint probability density function of velocity and scalars in turbulent flow, *Phys. Fluids* 24 (1981) 588–596.
- [20] L.Y. Gicquel, P. Givi, F.A. Jaber, S.B. Pope, Velocity filtered density function for large eddy simulation of turbulent flows, *Phys. Fluids* 14 (2002) 1196–1213.
- [21] M. Lee, R.D. Moser, Direct numerical simulation of turbulent channel flow up to $Re_\tau \approx 5200$, *J. Fluid Mech.* 774 (2015) 395–415.
- [22] S. Navarro-Martinez, T.-H. Un, M. Patel, Cerisse: A high-order LES/DNS solver for compressible turbulent reactive flows, <https://github.com/salvadornm/cerisse>.
- [23] W. Zhang, A. Almgren, V. Beckner, J. Bell, J. Blaschke, C. Chan, M. Day, B. Friesen, K. Gott, D. Graves, M.P. Katz, A. Myers, T. Nguyen, A. Nonaka, M. Rosso, S. Williams, M. Zingale, AMReX: a framework for block-structured adaptive mesh refinement, *J. Open Source Softw.* 4 (2019) 1370.
- [24] L. Fu, X.Y. Hu, N.A. Adams, A family of high-order targeted ENO schemes for compressible-fluid simulations, *J. Comput. Phys.* 305 (2016) 333–359.
- [25] E.F. Toro, M. Spruce, W. Speares, Restoration of the contact surface in the HLL-Riemann solver, *Shock Waves* 4 (1994) 25–34.
- [26] M.T.H. de Frahan, L. Esclapez, J. Rood, N.T. Wimer, P. Mullooney, B.A. Perry, L. Owen, H. Sitaraman, S. Yellapantula, M. Hassanaly, M.J. Rahimi, M.J. Martin, O.A. Doronina, S.N. A., M. Rieth, W. Ge, R. Sankaran, A.S. Almgren, W. Zhang, J.B. Bell, R. Grout, M.S. Day, J.H. Chen, The pele simulation suite for reacting flows at exascale, in: Proceedings of the 2024 SIAM Conference on Parallel Processing for Scientific Computing, 2024, pp. 13–25.
- [27] D. Modesti, S. Pirozzoli, Reynolds and Mach number effects in compressible turbulent channel flow, *Int. J. Heat Fluid Fl.* 59 (2016) 33–49.
- [28] F. Nicoud, F. Ducros, Subgrid-scale stress modelling based on the square of the velocity gradient tensor, *Flow Turbul. Combust.* 62 (1999) 183–200.
- [29] D.J. Micka, Combustion Stabilization, Structure, and Spreading in a Laboratory Dual-Mode Scramjet Combustor (Ph.D. thesis), University of Michigan, 2010.
- [30] C. Fureby, T. Nilsson, Large Eddy Simulation of cavity stabilized ramjet combustion, *Aerosp. Sci. Technol.* 141 (2023) 108503.
- [31] J. Li, Z. Zhao, A. Kazakov, F.L. Dryer, An updated comprehensive kinetic model of hydrogen combustion, *Int. J. Chem. Kinet.* 36 (2004) 566–575.
- [32] H. Sitaraman, S. Yellapantula, M.T.H. de Frahan, B. Perry, J. Rood, R. Grout, M. Day, Adaptive mesh based combustion simulations of direct fuel injection effects in a supersonic cavity flame-holder, *Combust. Flame* 232 (2021) 111531.